Mean, Variability and the Most Predictable Patterns in CFS over the Tropical Atlantic Ocean

Zeng-Zhen Hu[1], Bohua Huang[1,2], and Kathy Pegion[1]
[1]*Center for Ocean-Land-Atmosphere Studies, Calverton, MD*
[2]*Department of Climate Dynamics, George Mason University, Fairfax, VA*

NOAA CTB - COLA
Joint Seminar
Dec. 10, 2007

(1) Model and Model Output

As a state-of-the-art coupled system, the National Centers for Environmental Prediction (NCEP) Climate Forecast System (CFS) is now being used at NCEP for operational seasonal climate predictions. It has been demonstrated that the CFS reproduces the major features of the El Niño-Southern Oscillation (ENSO) (Wang et al. 2006; Saha et al. 2006) and the Asian and Australian monsoon (Liang et al. 2008). The atmospheric component of the CFS has horizontal resolution of T62 and 64 vertical sigma levels. The oceanic component is configured from the version 3 of the Modular Ocean Model of Geophysical Fluid Dynamics Laboratory (Pacanowski and Griffies 1998). The ocean model has 40 levels vertically, with 27 of them in the upper 400 meters. The domain of the ocean model extends from 74°S to 64°N with a horizontal grid of 1°x1° poleward of 30°S and 30°N, and with gradually increased meridional resolution to 1/3° between 10°S and 10°N. The atmospheric and oceanic components exchange surface fluxes on a daily interval without flux adjustment.

The NCEP CFS hindcasts analyzed in this work were initialized in all calendar months from 1981 to 2003. In a given start month, 15 nine month predictions were produced. The oceanic initial conditions (ICs) were taken from the NCEP Global Ocean Data Assimilation (GODAS) (Behringer et al. 1998, Behringer and Xue 2004) analyses on 11th and 21st of lead-month 0 and 1st of lead-month 1 (Saha et al. 2006). The atmospheric ICs were from the NCEP reanalysis II (Kanamitsu et al., 2002). For each of the three chosen oceanic ICs, five atmospheric ICs from 2 days before to 2 days after at daily interval were chosen to form 15 ocean-atmosphere ICs. The details about the ICs were given in Saha et al. (2006) and Huang et al. (2007). The monthly mean of the 15 individual member predictions and their ensemble mean are available from the NCEP website at

http://nomad6.ncep.noaa.gov/cfs/monthly.

In addition, a 52-year coupled integration using CFS was conducted at the Center for Ocean-Land-Atmosphere Studies (COLA). The

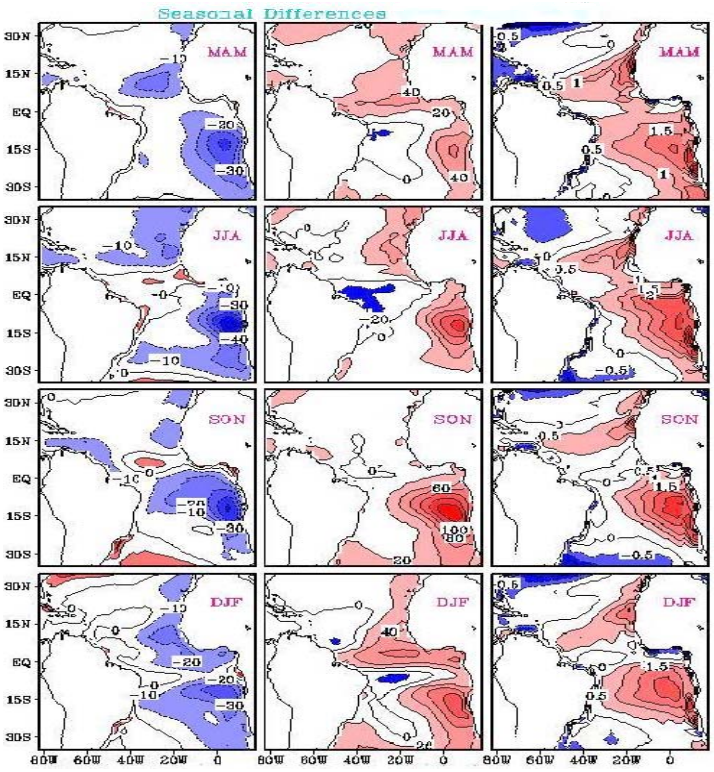

Figure 1 Seasonal mean climatology differences of low clouds (left column), downward short-wave radiation (central column), and SST (right column) between CFS simulation and corresponding analyses.

Correspondence to: Zeng-Zhen Wu, Center for Ocean-Land-Atmosphere Studies, 4041 Powder Mill Road, Suite 302, Calverton, MD 20705-3106. E-mail: hu@cola.iges.org

ocean-atmospheric IC is from January 1, 1985. The monthly data of the last 42 years, after a 10-year spin-up, are used in this analysis.

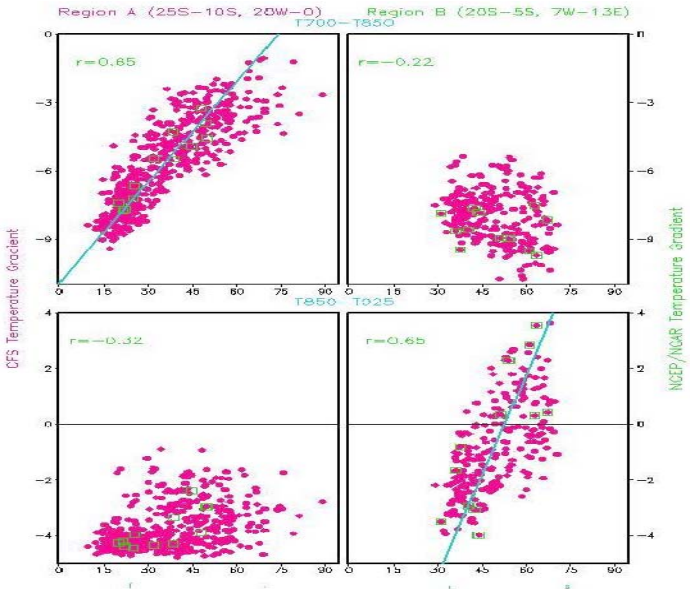

Figure 2 Scatter plot of low-level clouds (%) vs. T700-T850 (^{o}C, top panels), and vs. T850-T925 (^{o}C, bottom panels) averaged in the region of (25^{o}S-15^{o}S, 20^{o}W-0) in the CFS (left column) and in the region of (20^{o}S-5^{o}S, 7^{o}W-13^{o}E) in the observations (right column). The circles represent individual monthly mean.

Based on the results from the above CFS hindcasts and the long-term integration, we examined the model mean climate, variability (Hu et al. 2008a), leading modes and their physics (Hu et al. 2008b), as well as the predictive skill and the most predictable patterns (Hu and Huang 2007) in the tropical Atlantic. The main conclusions are listed in the following.

(2) **Mean Climate and Variability**

By comparing the CFS simulation with corresponding observation-based analyses/re-analyses, it is shown that the CFS captures the seasonal mean climate, including the zonal gradients of sea surface temperature (SST) in the equatorial Atlantic Ocean, even though the CFS produces warm mean biases and underestimates the variability over the southeastern ocean (right column of Fig. 1). It is also found that the CFS produces too few low-level clouds (left column of Fig. 1) and too many high-level clouds (not shown) over the southeastern part of the tropical Atlantic. The center of the low clouds in the model is also shifted westward, away from the cold tongue region, to the central ocean. The underestimation of low-level clouds in the southeastern Atlantic could be a cause of the warm SST biases in this region.

The low-level clouds are linked to a stable or inversion layer between 850 hPa and 925 hPa in the observation, but found to be associated with a stable layer between 700 hPa and 850 hPa in the CFS (Fig. 2). On average, the lower troposphere is less stable in the CFS than in the observation over the tropical Atlantic, a condition more favorable for the development of deeper convection. Moreover, in the observation, the low-level cloud variability in the South Atlantic is mainly associated with anomalies in the southeastern Atlantic and along the African coast, but in the CFS prediction the anomalies are moved to the subtropical South Atlantic.

Overall, the interactive processes among the low-level clouds, vertical inversion layer, and SST are important. The inadequate low-level cloud (left column of Fig. 1) and excessive short-wave radiation (central column of Fig. 1) are associated with the warm SST biases in the southeastern Atlantic (right column of Fig. 1). In return, the warm biases do not favor an inversion layer and low cloud formation (Fig. 2). Details about this part are given in Hu et al. (2008a).

(3) **Leading Modes and Physics**

The mean annual cycle, interannual variability, and leading patterns of the tropical Atlantic Ocean simulated in a long-term integration of CFS are examined (Hu et al. 2008b). Besides the warm biases in the tropical southeastern Atlantic, it is found that the seasonal transition from warm to cold phase along the equator is delayed one month in the CFS compared with the observations. This delay might be related to the failure of the model to simulate the cross-equatorial meridional wind associated with the African monsoon.

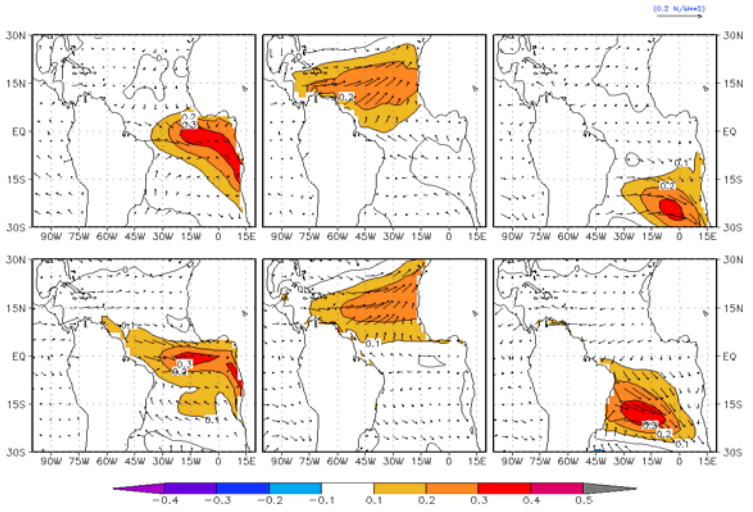

Figure 3 Spatial patterns (shading and contour) of REOFs of ERv2 (top panels) and the CFS simulated (bottom panels) seasonal mean SST in the tropical Atlantic (30°S-30°N, 100°W-20°E). The vectors represent the simultaneous regression of seasonal mean wind stress onto the corresponding time series of the REOF. The contour interval is 0.1°C. The percentages of the variance explained by each pattern are 16%, 15%, 10% (top panels from left to right), 10%, 11%, and 12% (bottom panels from left to right).

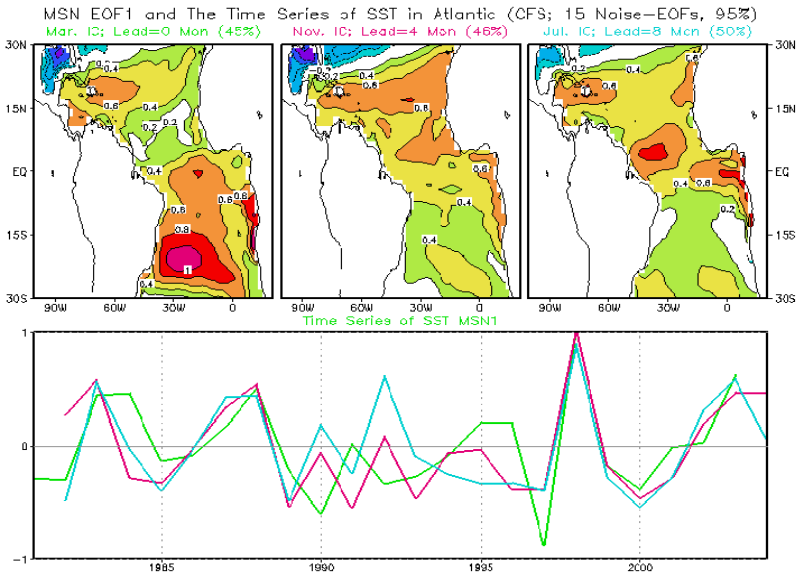

Figure 4 Spatial patterns (top panels) and time series (bottom panels) of MSN EOF1 of March SST, lead 0 month and March IC (top left), lead 4 months and November IC (top central), and lead 8 months and July IC (to right). The contour interval is 0.2, the zero lines are omitted, and the shading is for values larger than 0.2 or smaller than -0.2 for the spatial patterns. The real magnitude of the SST anomalies (°C) can be restored by multiplying the values in the spatial patterns with the corresponding time series. The percentage of the explained variance for the ensemble mean anomalies is indicated in each panel.

The CFS realistically simulates both the spatial structure and spectral distributions of the three major leading patterns of the SST anomalies in the tropical Atlantic Ocean: the south tropical Atlantic pattern (STA), the North tropical Atlantic pattern (NTA), and the southern subtropical Atlantic pattern (SSA) (Fig. 3). The CFS simulates the seasonal dependence of these patterns and partially reproduces their association with ENSO. The dynamical and thermodynamic processes associated with these patterns in the simulation and the observations are similar. The air-sea interaction processes associated with the STA pattern are well simulated in the CFS. The primary feature of the anomalous circulation in the Northern Hemisphere (NH) associated with the NTA pattern resembles that in the Southern Hemisphere (SH) linked with the SSA pattern, implying a similarity of the mechanisms in the evolution of these patterns and their connection with the tropical and extratropical anomalies in their respective hemispheres. The anomalies associated with both the SSA and NTA patterns are dominated by atmospheric fluctuations of equivalent-barotropic structure in the extratropics including zonally symmetric and asymmetric components. The zonally symmetric variability is associated with the annular modes, the Arctic Oscillation in the NH and the Antarctic Oscillation in the SH. The zonally asymmetric part of the anomalies in the Atlantic is teleconnected with the anomalies over the tropical Pacific. The misplaced teleconnection center over the southern subtropical ocean may be one of the reasons for the deformation of the SSA

pattern in the CFS.

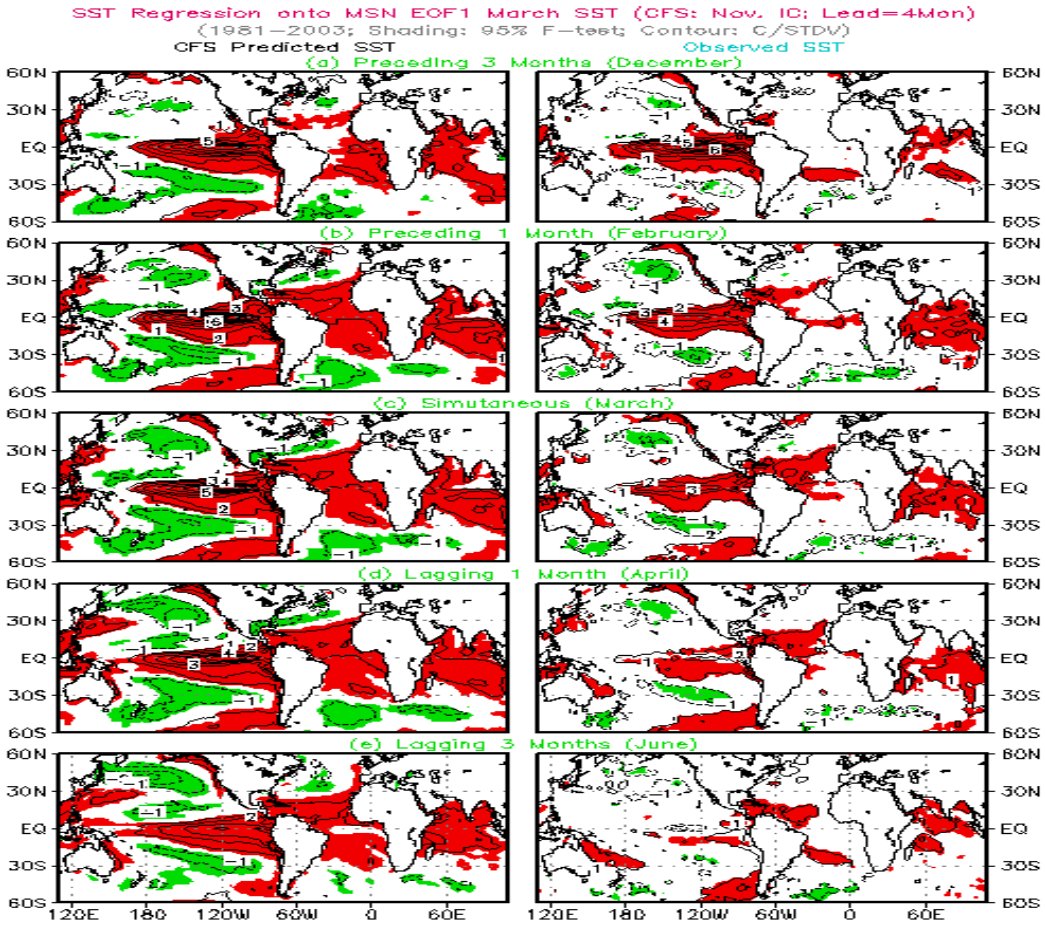

Figure 5 CFS predicted (left column) and OIv2 analyzed (right column) SST regression onto SST MSN EOF1 time series for lead 4 months and November IC (Fig. 4) at different leading and lagging months. The contour interval is 1.0°C per standard deviation of the MSN EOF1 time series, the zero lines are omitted, and the shading indicates the significance of the regression at the 95% confidence level**.**

(4) **Predictive Skill and Most predictable Patterns**

The predictive skill and most predictable patterns in the tropical Atlantic Ocean are studied using the CFS hindcasts (Hu and Huang 2007). The skill is measured by SST anomaly correlation between the predictions and the corresponding analyses. On average, for predictions with IC of all months, the predictability of SST is higher in the west than in the east. The highest skill is near the tropical Brazilian coast and in Caribbean Sea, and the lowest skill occurs in the eastern coast. Seasonally, the skill is higher for predictions with IC in summer or autumn and lower for those with IC in spring. CFS poorly predicts the meridional gradient in the tropical Atlantic Ocean. The superiority of the CFS predictions to the persistence forecasts depends on IC month, region, and lead-time. The CFS prediction is generally better than the corresponding persistence forecast when lead-time is longer than 3 months.

The predictable patterns are identified by applying an empirical orthogonal function (EOF) analysis with maximized signal-to-noise ratio (MSN EOF hereafter) to the predicted time series of 1981-2003 with given lead-time of the hindcasts. The most predictable pattern of SST in March has the same sign in almost the whole tropical Atlantic (Fig. 4). The corresponding pattern of geopotential height at 200 hPa (H200) is dominated by the same sign in most of the domain, while the corresponding precipitation pattern showed a distinct opposite

variation between the northwestern tropical North Atlantic and the regions from tropical South America to the southwestern tropical North Atlantic (not shown). The time series of the most predictable pattern of SST (Fig. 4), as well as the H200 and precipitation, are highly correlated with the SST in the eastern tropical Pacific (Fig. 5), implying that the predictable signals mainly result from the ENSO influence. The significant values in the most predictable precipitation pattern in the regions from tropical South America to the southwestern tropical North Atlantic in March are associated with the regional excessive divergence (convergence) at low (high) level in the CFS hindcast. Due to the strong connection between ENSO and the most predictable patterns in the tropical Atlantic in the model, the predictive skill of the CFS in the tropical Atlantic is largely determined by its ability to predict ENSO. The relative high predictive skill of the tropical North Atlantic SST is consistent with the CFS ability of predicting ENSO on interseasonal time scales, particularly for the ICs in warm months from March to October. In the southeastern ocean, the systematic warm bias is considered as a crucial factor causing the low skill in that region.

Acknowledgements We appreciate the suggestions and comments of Drs. S. Saha, S. Yang, K. Campana, and Mr. B. Jha.

References:

Behringer, D., M. Ji, A. Leetmaa, 1998: An improved coupled model for ENSO prediction and implications for ocean initialization. Part I: The ocean data assimilation system. *Mon. Wea. Rev.*, **126,** 1013-1021.

Behringer, D., and Y. Xue, 2004: Evaluation of the global ocean data assimilation system at NCEP: The Pacific Ocean. *Eighth Symposium on Integrated Observing and Assimilation Systems for Atmosphere, Ocean, Land Surface*. *AMS 84th Annual Meeting*, Seattle, Washington, January 11-15, 2004.

Hu, Z.-Z., B. Huang, and K. Pegion, 2008a: Low cloud errors over the southeastern Atlantic in the NCEP CFS and their association with lower-tropospheric stability and air-sea interaction. J. Geophys. *Res. (Atmosphere)* (submitted).

Hu, Z.-Z., B. Huang, and K. Pegion, 2008b: Leading patterns of the tropical Atlantic variability in a coupled general circulation model. *Clim. Dyn.,* DOI 10.1007/s00382-007-0318-x (in press).

Hu, Z.-Z. and B. Huang, 2007: The predictive skill and the most predictable pattern in the tropical Atlantic: The effect of ENSO. *Mon. Wea. Rev.*, **135 (5),** 1786-1806.

Huang, B., Z.-Z. Hu, and B. Jha, 2007: Evolution of model systematic errors in the tropical Atlantic basin from the NCEP coupled hindcasts. *Clim. Dyn*., **28 (7/8),** 661-682, DOI 10.1007/s00382-006-0223-8.

Kanamitsu, M., W. Ebisuzaki, J. Woollen, S.-K. Yang, J. J. Hnilo, M. Fiorino, and G. L. Potter, 2002: NCEP-DOE AMIP-II Reanalysis (R-2). *Bull. Amer. Meteor. Soc.*, **83**, 1631-1643.

Liang, J., S. Yang, Z.-Z. Hu, B. Huang, A. Kumar, and Z. Zhang, 2007: Predictable patterns of the Asian and Indo-Pacific summer climate in NCEP CFS. *Clim. Dyn.*, (revised).

Pacanowski, R. C., and S. M. Griffies, 1998: MOM 3.0 manual, NOAA/Geophysical Fluid Dynamics Laboratory, Princeton, New Jersey, USA 08542, 668 pp.

Saha, S, S. Nadiga, C. Thiaw, J. Wang, W. Wang, Q. Zhang, H. M. van den Dool, H.-L. Pan, S. Moorthi, D. Behringer, D. Stokes, M. Pena, S. Lord, G. White, W. Ebisuzaki, P. Peng, and P. Xie (2006), The NCEP climate forecast system. *J. Climate*, **19,** 3483-3517.

Wang, W., S. Saha, H.-L. Pan, S. Nadiga, and G. White, 2005: Simulation of ENSO in the new NCEP coupled forecast system model. *Mon. Wea. Rev.*, **133,** 1574-1593.